HHS Public Access

Author manuscript

Bioorg Med Chem. Author manuscript; available in PMC 2019 July 31.

Published in final edited form as:

Bioorg Med Chem. 2017 June 15; 25(12): 2995–3005. doi:10.1016/j.bmc.2017.03.048.

Small molecules inhibit STAT3 activation, autophagy, and cancer cell anchorage-independent growth

Donghui Zhou[a], **Maya Z. Springer**[b], **David Xu**[c,d], **Degang Liu**[a], **Andy Hudmon**[a], **Kay F. Macleod**[b], **Samy O. Meroueh**[a,c,*]

[a]Department of Biochemistry and Molecular Biology, Indiana University School of Medicine, United States

[b]The Ben May Department for Cancer Research, University of Chicago, United States

[c]Center for Computational Biology and Bioinformatics, Indiana University School of Medicine, United States

[d]Department of BioHealth Informatics, Indiana University School of Informatics and Computing, United States

Abstract

Triple-negative breast cancers (TNBCs) lack the signature targets of other breast tumors, such as HER2, estrogen receptor, and progesterone receptor. These aggressive basal-like tumors are driven by a complex array of signaling pathways that are activated by multiple driver mutations. Here we report the discovery of **6** (KIN-281), a small molecule that inhibits multiple kinases including maternal leucine zipper kinase (MELK) and the non-receptor tyrosine kinase bone marrow X-linked (BMX) with single-digit micromolar IC_{50}s. Several derivatives of **6** were synthesized to gain insight into the binding mode of the compound to the ATP binding pocket. Compound **6** was tested for its effect on anchorage-dependent and independent growth of MDA-MB-231 and MDA-MB-468 breast cancer cells. The effect of **6** on BMX prompted us to evaluate its effect on STAT3 phosphorylation and DNA binding. The compound's inhibition of cell growth led to measurements of survivin, Bcl-X_L, $p21^{WAF1/CIP1}$, and cyclin A2 levels. Finally, LC3B-II levels were quantified following treatment of cells with **6** to determine whether the compound affected autophagy, a process that is known to be activated by STAT3. Compound **6** provides a starting point for the development of small molecules with polypharmacology that can suppress TNBC growth and metastasis.

1. Introduction

Triple-negative breast cancer (TNBC) has taken on added importance in recent years as it is characterized by poor prognosis, aggressive behavior, and a lack of specific targets such as

*Corresponding author at: Department of Biochemistry and Molecular Biology, Indiana University School of Medicine, Van Nuys Medical Science Building, MS 4023, 635 Barnhill Drive, Indianapolis, IN 46202-5122, United States. smeroueh@iu.edu (S.O. Meroueh).

Disclosure of potential conflicts of interest

No potential conflicts of interest were disclosed.

ER, HER2, or progesterone receptor. Although chemotherapy is effective for TNBC patients in the adjuvant setting, chemotherapy-resistant TNBC is quickly fatal given its rapid growth and lack of targeted therapies. TNBC accounts for approximately 15% of breast cancer cases in the United States. Despite its lower incidence, TNBC contributes disproportionately to breast cancer morbidity and mortality compared to other breast cancer subtypes. This can be attributed in part to its intrinsic aggressiveness, but much of the excess mortality is due to the absence of effective targeted therapies. New targets and small molecules to probe these targets are needed for the development of effective therapeutic agents for the treatment of TNBC.[1]

Unlike other subtypes of cancer, hormone therapy or biologics such as trastuzumab have little effect on TNBC tumors. There is currently an intense search for vulnerabilities of this breast cancer sub-type that can be exploited for the development of targeted therapeutic agents. To identify new targets that suppress growth and metastasis of TNBC tumors, we previously screened a commercial library of small molecules using structure-based molecular docking. The focus was on members of the CaMK superfamily of kinases, which are relatively unexplored in cancer. We identified **1**, a small molecule that inhibited CaMKIIδ with single-digit micromolar IC_{50}s. Kinome-wide profiling against 337 kinases confirmed that CaMKIIδ was among the top 10 targets of the compound, along with other members of the CaMK family, such as the maternal embryonic zipper leucine kinase (MELK), and the non-receptor tyrosine kinase bone marrow X-linked (BMX).

The inhibition of multiple kinases by **1** prompted us to explore the compound and several of its derivatives in TNBC breast cancer cell lines MDA-MB-468 and MDA-MB-231. We focused on **6** (KIN-281). The compound was tested for activity in a panel of 25 kinases. We explored the effects of the compound on cell viability and colony formation in anchorage-dependent and independent assays. We further explored the effect of compounds on pro-apoptotic survivin and Bcl-X_L, as well as cell cycle protein cyclin-dependent kinase inhibitor 1 ($p21^{WAF1/CIP1}$). Considering the effect on BMX and Bcl-X_L we examined the effects of the compound on signal transducer and activator of transcription 3 (STAT3) as well as autophagy, which is activated by STAT3.

2. Materials and methods

2.1. Cell culture

MDA-MB-231 or MDA-MB-468 cells were cultured in Dulbecco's Modified Eagle Medium (Cellgro, Manassas, VA) supplemented with 10% FBS, 1% penicillin/streptomycin in a 5% CO_2 atmosphere at 37 °C.

2.2. Cell viability assay

MDA-MB-231 (10^4 cells) were plated overnight in 100 ml in each well of 96-well plates, and then treated with 1% DMSO (control) or compounds at the indicated concentrations for 3 d. 20 μl of 5 mg/ mL MTT (Sigma-Aldrich, St. Louis, Missouri) were added to each well, and cells were incubated at 37 °C in 5% CO_2 for 2 h. Viable cells were quantified at absorbance of 570 and 630 nm (reference background). Glioma cells were seeded into 96-

well plates and treated with KIN compounds. After 5 d of incubation, cell growth was determined by methylene blue staining. Each experiment was conducted in triplicate and repeated three times.

2.3. Western blot analysis

Anti-β-actin was obtained from Santa Cruz Biotechnology (CA, USA). Anti-LC3B was obtained from Sigma chemicals Co (St. Louis, MO, USA). Anti-p21, cyclin A2, anti-p53, anti-phospho p53 (Ser^{15}), MDMX, anti-phosphor STAT3 (Tyr^{705}), anti-STAT3, anti-Bcl-X_L, anti-survivin, anti-β-catenin, anti-phospho Akt, anti-E-cadherin, were obtained from Cell Signaling Technology (Beverly, MA, USA). Total cell lysates were prepared in standard RIPA extraction buffer containing protease and phosphatase inhibitors (Sigma-Aldrich, St. Louis, Missouri). Thirty micrograms of protein were separated by 10% SDS-PAGE and transferred to nitrocellulose membranes (Amersham, Arlington Heights, IL). The membranes were immunoprobed with primary antibodies at 4 °C overnight separately, followed by secondary antibody IRDye 800-conjugated goat anti-mouse IgG (Rockland, Immunochemicals, Gibertsville, PA) or Alexa Fluor 680 goat anti-rabbit IgG (Life Technologies, Grand Island, NY) for 1 h at room temperature. Bands were detected using Li-Cor Odyssey Imaging System (Li-Cor, Lincoln, NE).

2.4. Soft agar assay for colony formation

0.5 mL base layer of 0.5% agar in DMEM medium containing 10% fetal bovine serum was placed in 24-well plates and permitted to solidify at room temperature. Cells to be tested for colony formation were suspended in the top layer (0.5 mL) of 0.3% agar in DMEM medium with 10% fetal bovine serum. The agar was permitted to solidify at room temperature. 0.25 mL feeding medium was added on the top layer with 1% DMSO (control) or compounds at the indicated concentrations for 10 d at 37 °C in a humidified incubator in an atmosphere of 5% CO_2. The feeding medium was change twice a week. Cell colonies were stained with 0.005% Crystal Violet and inspected with a dissecting microscope.

2.5. Electrophoresis mobility shift assay (EMSA)

STAT3 consensus oligonucleotides (Santa Cruz, Dallas, TX) were first labeled with [γ^{32}P]-ATP by using polynucleotide kinase (Sigma Aldrich, St. Louis, MO). A total of 2 μg of nuclear protein was incubated with ^{32}P-labeled STAT3 probe in binding buffer (10 mM Tris, 50 mM KCl, 1 mM DTT, pH 7.5, 50 ng/μL Poly (dIdC), 50 μM EDTA pH 7.5) for 30 min on ice. After incubation, the samples were separated on 4% native polyacrylamide gel containing 50 mM Tris, pH 7.5, 0.38 M glycine and 2 mM EDTA. The gel was transferred to Whatman paper, covered with saran wrap and dried at 80 °C in vacuum dryer for 1–2 h. ^{32}P-labeled bands were visualized by autoradiography.

2.6. Autophagy assays

Bafilomycin A1 (Enzo) was added at 100 nM for 4 h before harvest of cells. Cells were lysed in NP40 buffer (150 mM NaCl, 50 mM Tris-HCl pH 7.5, 1 mM EDTA, 1% NP40) with protease and phosphatase inhibitors. Lysates were centrifuged at 16,300g for 15 min at 4 °C; supernatants were separated by SDS-PAGE. After transfer to PVDF, membranes were

blocked in 5% milk/PBS for 1 h at RT and incubated at 4 °C overnight with primary anti-LC3B antibody from Novus (cat# NB600–1384) at 1:3000 in 5% milk/PBS. Membranes were washed 3× in PBS-T 0.05% Tween and then incubated for 2 h with secondary (anti-rabbit HRP, 1:10,000) at RT. Membranes were washed 2× in PBS-T 0.05% Tween. Detection was performed by enhanced chemiluminescence after 2-h incubation with HRP-conjugated secondary antibodies (Dako).

2.7. Virtual screening

The program Glide from Schrödinger (Schrödinger LLC, New York, NY, 2016) was used for molecular docking of **6** to the MELK ATP binding pocket. Glide is a robust docking program that has been extensively validated in previous studies. The structures of **6** was prepared using LigPrep in Schrödinger. Compound was protonated at pH 7. The structure of MELK (PDB ID: 4CQG, 2.57 Å) was prepared for docking. A grid box was generated for the MELK structure for docking in Glide, with a box size of 21 Å and an inner box of 14 Å. All other parameters were set to default values. A series of binding poses were generated by docking **6** and its derivatives against the ATP binding site of MELK using Glide in standard precision (SP) mode. All other parameters were left to default values.

2.8. General synthesis methods

All chemicals were purchased from either Sigma-Aldrich or Acros Organics. Column chromatography was carried out with silica gel G (25–63 μm). Mass Spectra were measured on an Agilent 6520 Mass Q-TOF instrument. ^{1}H NMR and ^{13}C NMR spectra were recorded on BRUKER 500 MHz or 400 MHz spectrometer, using TMS as an internal standard and $CDCl_3$ or DMSO-d_6 as solvents. Chemical shifts (δ values) and coupling constants (J values) are reported in ppm and hertz, respectively. Anhydrous solvent and reagents were all analytically pure and dried through routine protocols. All compounds that were evaluated in biological essays had >95% purity verified by HPLC.

2.8.1. 2-Methyl-6-nitroquinazolin-4(3H)-one (6a)—2-Amino-5-nitro benzoic acid (1.821 g, 10.0 mmol) was added to acetic anhydride (60 mL). The mixture was stirred at 110 °C for 5 h. The mixture was evaporated to dryness under reduced pressure. The residue was mixed with ammonium hydroxide solution (20–28% NH_3 in H_2O, 60 mL) and the mixture was stirred at 55 °C for 10 h. The suspension was cooled to 5 °C, and the precipitate was filtered and washed with water. The filter cake was dried under vacuum pressure to give the desired product as a bright yellow solid (1.560 g, 76% yield). ^{1}H NMR (500 MHz, DMSO-d_6) δ 8.74 (d, J = 2.5 Hz, 1H), 8.48–8.50 (dd, J = 2.5, 9 Hz, 1H), 7.73 (d, J = 9 Hz, 1H), 2.41 (s, 3H); ^{13}C NMR (125 MHz, DMSO-d_6) δ 160.9, 158.6, 153.1, 144.3, 128.2, 128.2, 121.8, 120.5; HRMS (ESI) *m/z*: calcd for $C_9H_8N_3O_3Na$ $[M+Na]^+$ 228.0385, found 228.0372.

2.8.2. 2, 4, 6-Trichlorobenzaldehyde (6b)—1, 3, 5-Trichlorobenzene (1.81 g, 10 mmol) was dissolved in anhydrous THF (36 mL) and the mixture was stirred at −78 °C. *n*-BuLi (1.6 M in Hexane) (6.3 mL, 10 mmol) was slowly added into the solution over 0.5 h under −78 °C. The solution became light yellow color. After all the *n*-BuLi was added, the mixture was kept at −78 °C and stirred for 0.5 h then anhydrous DMF (1.32 mL, 17 mmol)

was added into the mixture dropwise and the resulting light yellow solution was continuously stirred at −78 °C for another 1.5 h. The reaction was quenched with 3 N HCl solution (36 mL) while kept the flask at −78 °C and warmed to ambient temperature to afford a colorless solution. The mixture was extracted with ethyl acetate (20 mL × 3) and the organic layer was then washed with saturated $NaHCO_3$ (aq) and brine, respectively. The organic layer was dried over anhydrous $MgSO_4$ and concentrated to afford product **6b** as a white needle like solid (1.99 g, 96%). ^{1}H NMR (500 MHz, $CDCl_3$) δ 10.43 (s, 1H), 7.42 (s, 2H); ^{13}C NMR (125 MHz, $CDCl_3$) δ 187.7, 139.4, 137.8, 130.0, 128.8. HRMS (ESI) *m/z:* calcd for $C_7H_4Cl_3O$ $[M+H]^+$ 208.92, found 208.9.

2.8.3. 6-Nitro-2-(2, 4, 6-trichlorostyryl)quinazolin-4(3H)-one (6c)—A solution of **6a** (205 mg, 1 mmol) and **6b** (210 mg, 1 mmol) in acetic acid (3 mL) was refluxed for 30 h. The mixture was cooled to room temperature, and the precipitate was filtered and washed with methanol (2 mL × 3). The filter cake was collected to give the desired product as a yellow solid (329 mg, 83% yield). ^{1}H NMR (500 MHz, DMSO-d_6) δ 8.77 (s, 1H), 8.25 (m, 1H), 7.82 (m, 1H), 7.75 (s, 2H), 7.55 (s, 1H), 6.99 (m, 1H). HRMS (ESI) *m/z:* calcd for $C_{16}H_9C_{13}N_3O_3$ $[M+H]^+$ 395.96, found 396.0.

2.8.4. N^1,N^1-diethyl-N4-(6-nitro-2-(2,4,6-trichlorostyryl)quinazolin-4-yl)pentane-1,4-diamine (6d)—A solution of **6c** (397 mg, 1.0 mmol) and DIEA (0.4 mL) in $POCl_3$ (10 mL) was refluxed for 3 h. The mixture was cooled to room temperature and concentrated to remove the solvent. The residue was added ice-water, and adjusted pH to 9–10 with saturated solution of Na_2CO_3. The mixture was extracted with EA (10 mL × 3). The combined organic phases were dried with anhydrous Na_2SO_4, filtered and concentrated. The residue was purified by column chromatography (PE/EA = 4:1) to give the desired product as a light brown solid (274 mg, 66% yield). HRMS (ESI) *m/z:* calcd for $C_{16}H_8$-$Cl_4N_3O_2$ $[M+H]^+$ 413.93, found 413.9.

2.8.5. (E)-N^1,N^1-diethyl-N^2-(6-nitro-2-(2,4,6-trichlorostyryl) quinazolin-4-yl)propane-1,2-diamine (6e)—Compound **6d** (415 mg, 1 mmol) was dissolved in THF (15 mL) and the solution was added N^1,N^1-diethylpentane-1,4-diamine (316 mg, 2.0 mmol). The reaction mixture was stirred at room temperature for 3 h. The mixture was diluted with EA (60 mL). It was washed with water and saturated solution of NH_4Cl. Then the organic layer was dried by anhydrous Na_2SO_4 and the solvents were removed at reduced pressure. After purified by flash column chromatography (30:1, $CHCl_3$/CH_3OH), compounds **6e** (301 mg, yield 56%) was got as a golden yellow solid. ^{1}H NMR (500 MHz, DMSO-d_6) 9.01 (s, 1H), 8.42–8.44 (dd, J = 2.0, 9.0 Hz, 1H), 8.19 (d, J =16.0 Hz, 1H), 7.88 (d, J = 6.5 Hz, 1H), 7.83 (d, J = 9.5 Hz, 1H), 7.41 (s, 2H), 7.33 (d, J =16.0 Hz, 1H), 4.59–4.60 (m, 1H), 2.81–2.82 (m, 4H), 2.69 (m, 3H), 2.03–2.05 (m, 1H), 1.82 (m, 3H), 1.42 (d, J = 6.5 Hz, 3H), 1.16 (t, J = 7.0 Hz, 6H); ^{13}C NMR (125 MHz, DMSO-d_6) δ 163.2, 159.9, 154.4, 144.2, 137.1, 135.6, 134.0, 132.4, 132.0, 129.7, 128.9, 126.4, 119.7, 113.7, 52.7, 51.0, 47.5, 34.1, 22.9, 20.3, 10.4; HRMS (ESI) *m/z:* calcd for $C_{25}H_{28}Cl_3N_5O_2$ $[M+H]^+$ 536.1381, found 536.1404.

2.8.6. (E)-N^4-(5-(diethylamino)pentan-2-yl)-2-(2,4,6-trichlorostyryl) quinazoline-4,6-diamine (6)—To a solution of **6e** (310 mg, 0.58 mmol) in MeOH/H_2O

(1:1, 22 mL) was added ammonium chloride (310 mg, 5.8 mmol) and Fe powder (167 mg, 2.99 mmol). The resulting solution was reluxed for 4 h and monitored (by LCMS) for the conversion to the corresponding aniline. The reaction was then filtered and the solvent was removed *in vacuo*. After cooling to room temperature, the mixture was filtered through a pad of Celite which was washed with MeOH and the filtrate was concentrated *in vacuo*. The crude residue was adjusted to pH 7 by saturated $NaHCO_3$ solution and extracted with $CHCl_3$. The combined $CHCl_3$ layer was then washed with brine, dried over anhydrous $MgSO_4$ and solvent was removed *in vacuo*. The resulting crude residue was purified by flash column chromatography (loaded using DCM/Hexane, 1:5 then eluted with $CHCl_3$(NH_4OH saturated)/MeOH, 10:1) and dried under high vacuum to afford the desired product **6** (205 mg, 70%) as red solid. ^1H NMR (400 MHz, $CDCl_3$) δ 8.56 (s, 1H), 8.06–8.02 (d, J = 16.0 Hz, 1H), 7.69–7.66 (d, J = 8.8 Hz, 1H), 7.46–7.42 (m, 1H), 7.39–7.38 (m, 3H), 7.13–7.07 (m, 1H), 4.62 (m, 1H), 3.08–2.94 (m, 6H), 20.2–1.78 (m, 4H), 1.40–1.39 (d, J = 6.4 Hz, 3H), 1.25–1.22 (t, 6H); ^{13}C NMR (100 MHz, $CDCl_3$): δ 168.9, 157.7, 156.9, 144.9, 143.8, 137.8, 135.2, 133.0, 132.9, 129.6, 128.6, 128.1, 122.9, 115.4, 103.2, 55.1, 46.5, 46.4, 33.5, 22.0, 20.8, 9.2. HRMS (ESI) *m/z:* calcd for $C_{25}H_{31}Cl_3N_5$ $[M+H]^+$ 506.16, found 506.1.

2.8.7. (E)-N^1,N^1-diethyl-N^2-(6-nitro-2-(2,4,6-trichlorostyryl) quinazolin-4-yl)propane-1,2-diamine (17a)—Compound **17a** (95 mg, 59.3%yield) was prepared by the same method as **6e**. HRMS (ESI) *m/z:* calcd for $C_{23}H_{25}Cl_3N_5O_2$ $[M+H]^+$ 508.10, found 508.1.

2.8.8. (E)-N^4-(1-(diethylamino)propan-2-yl)-2-(2,4,6-trichlorostyryl) quinazoline-4,6-diamine (17)—Compound **17** (35 mg, 28% yield) was prepared by the same method as **6**. ^1H NMR (400 MHz, $CDCl_3$) δ 8.55 (s, 1H), 8.18–8.16 (d, J = 7.6 Hz, 1H), 7.95–7.91 (d, J =16.4Hz, 1H), 7.68–7.66 (d, J =8.8 Hz, 1H), 7.39 (s, 2H), 7.38–7.34 (d, J =16.0 Hz, 1H), 7.33–7.32 (m, 1H), 7.13–7.11 (m, 1H), 5.03 (m, 1H), 3.74–3.68 (m, 1 H), 3.17–3.06 (m, 5 H), 1.52–1.50 (d, J = 6.8 Hz, 3H), 1.31–1.27 (t, J =7.2 Hz, 6H); ^{13}C NMR (100 MHz, $CDCl_3$): δ 168.5, 157.9, 156.2, 145.3, 137.5, 135.2, 133.1, 132.7, 129.1, 128.7, 127.8, 123.3, 115.9, 104.1, 55.1, 46.6, 42.8, 18.9, 8.5. HRMS (ESI) *m/z:* calcd for $C_{23}H_{27}Cl_3N_5$ $[M+H]^+$ 478.13, found 478.1.

2.8.9. (E)-N^1,N^1-diethyl-N^4-(6-nitro-2-(2,4,6-trichlorostyryl) quinazolin-4-yl)butane-1,4-diamine (18a)—Compound **18a** (105 mg, 72% yield) was prepared by the same method as **6e**. HRMS (ESI) *m/z:* calcd for $C_{24}H_{27}Cl_3N_5O_2$ $[M+H]^+$ 522.12, found 522.1.

2.8.10. (E)-N^4-(4-(diethylamino)butyl)-2-(2,4,6-trichlorostyryl) quinazoline-4,6-diamine (18)—Compound **18** (65 mg, 66%yield) was prepared by the same method as **6**. ^1H NMR (400 MHz, $CDCl_3$) δ 11.49 (br, 1H), 9.16 (br, 1H), 8.11–8.07 (d, J =16.0 Hz, 1H), 7.50–7.45 (m, 1H), 7.43–7.42 (m, 2H), 7.35 (s, 2H), 6.95–6.94 (d, J = 7.6 Hz, 1H), 3.75 (br, 2H), 3.14 (br, 6H), 1.97 (m, 2H), 1.87 (m, 2H), 1.34 (t, J = 6.8 Hz, 6H); ^{13}C NMR (100 MHz, $CDCl_3$): δ 158.6, 152.1, 148.2, 135.9, 135.2, 134.7, 129.8, 129.6, 129.1, 126.8, 124.0, 120.5, 114.1, 104.5, 51.4, 46.5, 40.9, 25.0, 21.3, 8.3. HRMS (ESI) *m/z:* calcd for $C_{24}H_{29}Cl_3N_5$ $[M+H]^+$ 492.14, found 492.1.

2.8.11. (E)-N^1,N^1-diethyl-N^3-(6-nitro-2-(2,4,6-trichlorostyryl) quinazolin-4-yl)butane-1,3-diamine (19a)—Compound **19a** (85 mg, 62% yield) was prepared by the same method as **6e**. HRMS (ESI) *m/z:* calcd for $C_{24}H_{27}Cl_3N_5O_2$ $[M+H]^+$ 522.12. found 522.1.

2.8.12. (E)-N^4-(4-(diethylamino)butan-2-yl)-2-(2,4,6-trichlorostyryl) quinazoline-4,6-diamine (19)—Compound **19** (25 mg, 31% yield) was prepared by the same method as **6**. ^{1}H NMR (400 MHz, $CDCl_3$) δ 8.06–8.02 (d, J=16.0 Hz, 1H), 7.75–7.69 (m, 2H), 7.46–7.42 (d, J=16.4 Hz, 1H), 7.38 (s, 2H), 7.14–7.15 (d, J= 9.2 Hz, 1H), 4.54–5.52 (m, 1H), 3.43–3.37 (m, 1H), 3.18–3.16 (m, 2H), 3.11–2.98 (m, 4H), 2.45–2.36 (m, 1H), 2.15–2.10 (m, 1H), 1.46–1.45 (d, J= 6.4 Hz, 3H), 1.33 (t, J=6.8 Hz, 3H); ^{13}C NMR (100 MHz, $CDCl_3$) δ 158.4, 155.7, 145.8, 135.6, 135.4, 133.4, 132.3, 129.3, 128.7, 127.5, 123.3, 115.5, 104.2, 49.6, 45.2, 30.7, 20.9, 8.3. HRMS (ESI) *m/z:* calcd for $C_{24}H_{29}Cl_3N_5$ $[M+H]^+$ 492.14, found 492.1.

2.8.13. 3-(2,4,6-Trichlorophenyl)propanoic acid (21a)—A mixture of **6b** (0.81 g, 3.87 mmol), 2,2-dimethyl-1,3-dioxane-4,6-dione (0.61 g, 4.26 mmol), triethylamine (780 mg, 7.72 mmol) and formic acid (0.87 g, 19.mmol) in DMF (20 mL) was stirred at 100 °C for 3 h. The mixture was cooled to room temperature and water was added (60 mL). The mixture was extracted with EA (25 mL × 2). The combined organic layers were washed with water and brine. The solution was dried with anhydrous Na_2SO_4, filtered and concentrated to give the desired product as a white solid (0.9 g, 92.4% yield). ^{1}H NMR (400 MHz, $CDCl_3$) δ 11.56 (br, 1H), 7.32 (s, 2H), 3.26–3.22 (t, J= 8.4 Hz, 2H), 2.63–2.59 (m, 2H). HRMS (ESI) *m/z:* calcd for $C_9H_6Cl_3O_2$ $[M-H]^-$ 250.95, found 250.9.

2.8.14. 6-Nitro-2-(2,4,6-trichlorophenethyl)quinazolin-4(3H)-one (21b)—A mixture of 3-(2,4,6-trichlorophenyl)propanoic acid (0.9 g, 3.6 mmol) in $SOCl_2$ (10 mL) was refluxed for 2 h. The mixture was concentrated to dryness to give 2-(2,4,6-trichlorophenyl) acetyl chloride (1.0 g, crude). To the acyl chloride was added drop-wise the solution of 2-amino-5-nitrobenzoic acid (0.65 g, 3.6 mmol) in pyridine (15 mL). The mixture was stirred at room temperature for 2 h. LC-MS showed the reaction was completed. The reaction was concentrated to remove the solvent and the residue was added acetic anhydride (20 mL). The mixture was stirred at 110 °C for 4 h. The mixture was evaporated to dryness under reduced pressure. The residue was mixed with ammonium hydroxide solution (20–28% NH_3 in H_2O) and the mixture was stirred at 60 °C for 2 h. The suspension was cooled to 5 °C, and the precipitate was filtered and washed with water. The filter cake was dried under vacuum pressure to give the desired product as a yellow solid (1.13 g, 79.8% yield). ^{1}H NMR (400 MHz, $CDCl_3$) δ 8.79–8.18 (d, J= 2.4 Hz, 1H), 8.49–8.46 (m, 1H), 7.75–7.73 (d, J= 8.8 Hz, 1H), 7.66 (s, 2H), 3.23–3.22 9 (m, 2H), 2.92–2.88 (t, J= 7.6 Hz, 2H). HRMS (ESI) *m/z:* calcd for $C_{16}H_{11}Cl_3N_3O_3$ $[M+H]^+$ 397.98, found 398.0.

2.8.15. 4-Chloro-6-nitro-2-(2,4,6-trichlorophenethyl)quinazoline (21c)—Compound **21c** (560 mg, 48% yield) was prepared by the same method as **6d**. HRMS (ESI) *m/z:* calcd for $C_{16}H_{10}Cl_4N_3O_2$ $[M+H]^+$ 415.94, found 415.9.

2.8.16. N^1,N^1-diethyl-N^4-(6-nitro-2-(2,4,6-trichlorophenethyl) quinazolin-4-yl)pentane-1,4-diamine (21d)—Compound **21d** (90 mg, 48% yield) was prepared by the same method as **6e**. HRMS (ESI) *m/z:* calcd for $C_{25}H_{31}Cl_3N_5O_2$ $[M+H]^+$ 538.14, found 538.1.

2.8.17. N^4-(5-(diethylamino)pentan-2-yl)-2-(2,4,6-trichlorophenethyl)quinazoline-4,6-diamine (21)—Compound **21** (90 mg, 48% yield) was prepared by the same method as **6**. ^{1}H NMR (400 MHz, $CDCl_3$) δ 8.70 (s, 1H), 7.62–7.60 (d, J=8.8 Hz, 1H), 7.30 (s, 2H) 7.26–7.24 (d, 2H), 7.12–7.09 (d, J= 9.2 Hz, 1H), 6.35 (br, 1H), 4.44 (m, 1H), 3.46–3.04 (m, 2H), 2.94–2.90 (m, 5H), 2.82–2.80 (m, 1H), 1.31–1.29 (d, J= 6.4 Hz, 3H), 1.22–1.18 (t, J=7.2 Hz, 6H); ^{13}C NMR (100 MHz, $CDCl_3$): δ 168.9, 161.9, 158.4, 144.5, 142.7, 136.9, 136.0, 132.1, 128.0, 128.0, 123.1, 114.4, 103.2, 51.9, 46.3, 37.1, 33.3, 29.8, 21.6, 20.8, 9.0. HRMS (ESI) *m/z:* calcd for $C_{25}H_{33}Cl_3N_5^+$ $[M+H]^+$ 508.17, found 508.1.

2.8.18. (E)-6-Nitro-2-(4-(trifluoromethyl)styryl)quinazolin-4(3H)-one (22a)—Compound **22a** (170 mg, 47% yield) was prepared by the same method as **6c**. HRMS (ESI) *m/z:* calcd for $C_{17}H_{11}F_3N_3O_3$ $[M+H]^+$ 362.07, found 362.1.

2.8.19. (E)-4-Chloro-6-nitro-2-(4-(trifluoromethyl)styryl)quinazoline (22b)—Compound **22b** (116 mg, 65% yield) was prepared by the same method as **6d**. HRMS (ESI) *m/z:* calcd for $C_{17}H_{10}ClF_3N_3O_2$ $[M+H]^+$ 380.03, found 380.0.

2.8.20. (E)-N^1,N^1-diethyl-N4-(6-nitro-2-(4-(trifluoromethyl)styryl) quinazolin-4-yl)pentane-1,4-diamine (22c)—Compound **22c** (crude 100 mg) was prepared by the same method as **6e**.The crude product was used in next step without further purification. HRMS (ESI) *m/z:* calcd for $C_{26}H_{31}F_3N_5O_2$ $[M+H]^+$ 502.24, found 502.2.

2.8.21. (E)-N^4-(5-(diethylamino)pentan-2-yl)-2-(4-(trifluoromethyl) styryl)quinazoline-4,6-diamine (22)—Compound **22** (70 mg, 75% yield) was prepared by the same method as **6**. ^{1}H NMR (400 MHz, $CDCl_3$) δ 8.26 (s, 1H), 7.90–7.86 (d, J=16.0 Hz, 1H), 7.71–7.60 (m, 5H), 7.39 (m, 1H) 7.32–7.28 (m, 1H), 7.13–7.10 (m, 1H), 6.75–6.74 (d, J=5.6 Hz, 1H), 4.68 (m, 1H), 3.05–2.99 (m, 5H), 2.976–2.91 (m, 1H), 1.98–1.82 (m, 4H), 1.40–1.38 (d, J= 6.4 Hz, 3H), 1.25–1.21 (t, J= 7.2 Hz, 6H); ^{13}C NMR (100 MHz, $CDCl_3$) δ 168.4, 158.1, 156.7, 145.3, 142.4, 140.3, 133.9,131.2, 130.0, 128.4, 127.4, 125.6, 125.6, 123.1, 115.3, 103.7, 51.7, 46.3, 46.2, 32.9, 21.2, 21.0, 8.3. HRMS (ESI) *m/z:* calcd for $C_{26}H_{33}F_3N_5$ $[M+H]^+$ 472.26, found 472.3.

2.8.22. (E)-6-Nitro-2-(3-(trifluoromethyl)styryl)quinazolin-4(3H)-one (23a)—Compound **23a** (286 mg, 40% yield) was prepared by the same method as **6c**. ^{1}H NMR (400 MHz, DMSO-d_6) δ 12.79 (s, 1H), 8.81 (d, J= 2.4 Hz, 1H), 8.56–8.53 (m, 1H), 8.16–8.12 (d, J=16.4 Hz, 1H), 8.045–8.00 (m, 2H), 7.86–7.82 (m, 2H), 7.74–7.71 (t, J= 7.6 Hz, 1H), 7.21–7.17 (d, J=16.0 Hz, 1H). HRMS (ESI) *m/z:* calcd for $C_{17}H_{11}F_3N_3O_3$ $[M+H]^+$ 362.07, found 362.1.

2.8.23. (E)-4-Chloro-6-nitro-2-(3-(trifluoromethyl)styryl)quinazoline (23b)— Compound **23b** (210 mg, 70% yield) was prepared by the same method as **6d**. HRMS (ESI) *m/z:* calcd for $C_{17}H_{10}ClF_3N_3O_2$ $[M+H]^+$ 380.03, found 380.0.

2.8.24. (E)-N^1,N^1-diethyl-N^4-(6-nitro-2-(3-(trifluoromethyl)styryl) quinazolin-4-yl)pentane-1,4-diamine (23c)—Compound **23c** (132 mg, 48% yield) was prepared by the same method as **6e**. HRMS (ESI) *m/z:* calcd for $C_{26}H_{31}F_3N_5O_2$ $[M+H]^+$ 502.24, found 502.2.

2.8.25. (E)-N4-(5-(diethylamino)pentan-2-yl)-2-(3-(trifluoromethyl) styryl)quinazoline-4,6-diamine (23)—Compound **23** (68 mg, 54% yield) was prepared by the same method as **6**. ^{1}H NMR (400 MHz, $CDCl_3$) δ 8.67 (s, 1H), 7.90–7.86 (d, J=15.6 Hz, 1H), 7.81(m, 2H), 7.68–7.65 (d, J= 8.8 Hz, 1H), 7.54–7.49 (m, 1H), 7.41–7.07 (m, 1H), 7.32–7.28 (d, J=15.6 Hz, 1H), 7.12–7.09 (m, 1H), 6.79 (br, 1H), 4.69 (m, 1H), 3.07–3.00 (m, 5H), 2.97–2.92 (m, 1H), 2.00–1.90 (m, 4H), 1.40–1.39 (d, J= 6.8 Hz, 3H), 1.25–1.22 (t, J= 7.2 Hz, 6H); ^{13}C NMR (100 MHz, $CDCl_3$) δ 168.8, 158.1, 156.3, 145.7, 141.6, 137.5, 134.1, 131.2, 130.9, 130.0, 129.2, 127.8, 125.4, 124.8, 124.3, 124.2, 123.2, 122.7, 115.2, 103.6, 51.7, 46.3, 46.1, 33.0, 21.2, 20.9, 8.4. HRMS (ESI) *m/z:* calcd for $C_{26}H_{33}F_3N_5$ $[M+H]^+$ 472.26, found 472.2.

2.8.26. (E)-6-Nitro-2-(2-(trifluoromethyl)styryl)quinazolin-4(3H)-one (24a)— Compound **24a** (306 mg, 42% yield) was prepared by the same method as **6c**. ^{1}H NMR (400 MHz, DMSO-d_6) δ 12.99 (s, 1H), 8.81 (d, J= 2.8 Hz, 1H), 8.55–8.52 (m, 1H), 8.34–8.31 (d, J= 14.0 Hz, 1H), 7.96–7.95 (d, J= 8.0 Hz, 1H), 7.90–7.80 (m, 3H, 7.69–7.65 (t, J= 7.6 Hz, 1H), 7.11–7.07 (d, J= 15.6 Hz, 1H). HRMS (ESI) *m/z:* calcd for $C_{17}H_{11}F_3N_3O_3$ $[M+H]^+$ 362.07, found 362.1.

2.8.27. (E)-4-Chloro-6-nitro-2-(2-(trifluoromethyl)styryl)quinazoline (24b)— Compound **24b** (80 mg, 64% yield) was prepared by the same method as **6d**. HRMS (ESI) *m/z:* calcd for $C_{17}H_{10}ClF_3N_3O_2$ $[M+H]^+$ 380.03, found 380.0.

2.8.28. (E)-N^1,N^1-diethyl-N^4-(6-nitro-2-(2-(trifluoromethyl)styryl) quinazolin-4-yl)pentane-1,4-diamine (24c)—Compound **24c** (80 mg, 57% yield) was prepared by the same method as **6e**. HRMS (ESI) *m/z:* calcd for $C_{26}H_{31}F_3N_5O_2$ $[M+H]^+$ 502.24, found 502.2.

2.8.29. (E)-N^4-(5-(diethylamino)pentan-2-yl)-2-(2-(trifluoromethyl) styryl)quinazoline-4,6-diamine (24)—Compound **24** (20 mg, 36% yield) was prepared by the same method as **6**. ^{1}H NMR (400 MHz, $CDCl_3$) δ 8.69 (s, 1H), 8.39–8.35 (m, 1H), 7.93–7.91 (d, J= 8.0 Hz, 1H), 7.69–7.64 (m, 2H), 7.58–7.54 (t, J= 7.6 Hz, 1H), 7.40–7.36 (t, J=7.6 Hz, 1H), 7.23–7.18 (d, J=15.6 Hz, 1H), 7.13–7.10 (m, 1H), 6.42 (br, 1H), 4.61 (m, 1H), 3.00–2.94 (m, 4H), 2.88–2.86 (m, 1H), 1.95–1.90 (m, 4H), 1.41–1.39 (d, J= 6.4 Hz, 3H), 1.22–1.19 (t, J= 7.2 Hz, 6H); ^{13}C NMR (100 MHz, $CDCl_3$) δ 157.8, 157.0, 145.1, 135.7, 132.5, 132.0, 131.0, 128.9, 127.7, 127.2, 126.0, 123.0, 15.4, 103.5, 51.7, 46.5, 46.1, 33.0, 21.3, 20.7, 8.5. HRMS (ESI) *m/z:* calcd for $C_{26}H_{33}F_3N_5$ $[M+H]^+$ 472.26, found 472.2.

3. Results

3.1. Compounds inhibit protein kinases

Previously, structure-based virtual screening against CaMKIIδ led to **1** (Scheme 1), which inhibited the enzyme with single-digit micromolar IC_{50}. Kinome profiling against 337 kinases of **4** (an analog of **1** with identical IC50) revealed that CaMKIIδ was among the top 10 targets of the compound. Also, the compound inhibited other members of CaMK family of proteins that included CaMKI and the maternal embryonic zipper kinase (MELK). To better understand how these compounds engage the ATP-binding pocket of kinases, we selected MELK to pursue a limited structure-activity study.

We purchased additional analogs of **1** (compounds **2**–**15**) and tested several compounds for inhibition of MELK (Fig. 1a). Compound **6** showed the most potent activity with more than 98% inhibition at 20 μM. To identify additional targets for **6**, we tested whether the compound inhibited the activity of the top 25 kinase targets of compound **1** that were identified from a previous profiling of 337 kinases (Fig. 1b). We found that **6** inhibits kinases with IC_{50} values ranging from 1.4 ± 0.9 μM for MELK to 42.7 ± 4.6 μM for FER kinase. Compound **6** inhibited two other kinases with an IC_{50} less than 2 μM, namely BMX/ETK (1.9 ±0.6 μM) and TIE2/TEK (1.8 ±0.9 μM).

To explore the role of each substituent of **6** on the inhibition of MELK activity, we prepared 9 derivatives of the compound (Scheme 2, 3, and Fig. 1c). The role of the amine at R_2 was investigated by replacing it with a methoxy group affording compound **16**. The compound was threefold weaker than **6** suggesting that the amino group was engaged in favorable interactions likely through hydrogen bonding (Fig. 1d). The role of the R_1 group was explored in compounds **17**, **18**, and **19**. In **17** and **19** the N-alkylmine moiety was shortened resulting in twofold increase in the IC_{50} over the parental compound. Removal of the methyl group at the carbon atom directly attached to the quinazoline ring in **18** led to little effect on the IC_{50}. An introduction of a morpholino group in **20** led to a twofold reduction in activity. The effect of the olefin at R_3 was explored by the synthesis of **21**. The loss of activity by nearly 3-fold suggests that a planar moiety at R1 is preferable for optimal binding to the kinase. This group interacts with sidechains of the hinge loop in the ATP-binding pocket of the enzyme (Fig. 1e). At R_3, a trifluoromethyl moiety was introduced at the *para* (compound **22**), *meta* (compound **23**), *ortho* (compound **24**) positions of the ring. Both **23** and **24** had 3-fold weaker activity than the parent compound, except for **22**, which resulted in a similar IC_{50}.

3.2. Compounds inhibit cancer cell growth in anchorage-dependent and independent assays

Considering that the kinases inhibited by the compound are known to be up-regulated in various basal-like breast tumors, we explored the effect of **1**–**15** on breast MDA-MB-231 cell viability (Fig. 2). Most of the compounds inhibited breast MDA-MB-231 cell growth with IC_{50} values that ranged from 2 to 30 μM (Fig. 2a). Except for **13** (KIN-288) and **12** (KIN-289), all compounds had IC_{50} values that were lower than 10 μM. The most potent compound was **6** (KIN-281) with an IC_{50} of 2 μM. We also explored the effect of the

compounds in anchorage-independent growth assay in soft agar. Colony formation in soft agar provides a better representation of oncogenic transformation, tumor growth, as well the potential for tumors to metastasize.[2] MDA-MB-231 cells form colonies in soft agar as illustrated in Fig. 2b and c. Compounds **1** (KIN-1), **4** (KIN-236), **6** (KIN-281) and **7** (KIN-283) inhibited colony formation in a concentration-dependent manner with IC_{50} values ranging from 3 to 7 μM. Consistent with cell viability studies, **6** (KIN-281) was generally more potent than the other three compounds.

3.3. Compounds Up-regulate p21$^{WAF1/CIP1}$ in a p53-dependent manner

Previous studies had shown that MELK contributes to cell cycle progression by causing G/M arrest,[3,4] and reduced the number of cells at the G_2/M transition.[4,5] These studies also showed that knockdown of MELK resulted in up-regulation of p21$^{WAF1/CIP1}$ in U87 GBM cell lines.[4] We observed the same effect for **1** (KIN-1) and **6** (KIN-281); at 5 μM, the compound up-regulated p21$^{WAF1/CIP1}$ in MDA-MB-468 (Fig. 3a and b) and MDA-MB-231 (Fig. 3c and d). A time-dependent study was conducted with both of these cell lines. After 4 h, both **1** (KIN-1) and **6** (KIN-281) up-regulate p21$^{WAF1/CIP1}$. The effect on p21$^{WAF1/CIP1}$ was sustained over 48 h in both cell lines. We investigated the effects of p21$^{WAF1/CIP1}$ on cyclins, which are inhibitors of p21$^{WAF1/CIP1}$. We found that an increase in p21$^{WAF1/CIP1}$ corresponded closely to a decrease in cyclin A2, which was gradually down-regulated over the course of 48 h (Fig. 3a–d).

Although p21$^{WAF1/CIP1}$ is a p53 target gene, treatment of MDA-MB-468 cells with **1** (KIN-1) and **6** (KIN-281) showed no effect on p53 levels over 48 h (Fig. 3e). We investigated whether the compounds had any effects on p53 phosphorylation, particularly at Ser15, which has been previously found to be affected by MELK suppression. Phosphorylation at Ser15 inhibits the interaction of p53 with its antagonists MDM2 or MDMX, which de-stabilize p53 and inhibit apoptosis. Interestingly, both compounds inhibited phosphorylation at Ser15 of p53 consistent with a potential effect on MELK activity (Fig. 3f).

3.4. Compounds block STAT3 and down-regulate pro-apoptotic markers survivin and Bcl-XL

Both **1** (KIN-1) and **6** (KIN-281) inhibited STAT3 phosphorylation in MDA-MB-468 (Fig. 4a and b) and MDA-MB-231 (Fig. 4c and d) cells. A time course revealed that STAT3 phosphorylation was completely inhibited at 4 h, but phosphorylation levels were restored after 8 h in MDA-MB-468 cells. A similar observation was made in MDA-MB-231 except that these cells recover STAT3 phosphorylation levels more slowly. The effect on STAT3 phosphorylation was confirmed with electrophoresis mobility shift assay (EMSA), which showed that **1** (KIN-1) inhibited STAT3 dimer binding to DNA (Fig. 4e). It is of interest to note that JAK kinase activity was not affected by our compounds as evidenced by the lack of inhibition of JAK kinase activity by **6** (Fig. 4f). This suggests that the inhibitors are following a non-canonical pathway to blocking STAT3. Previous studies have suggested that BMX promotes STAT3 activation through the PI3K pathway in a manner that is independent of Akt.[6] We find that **1** (KIN-1) or **6** (KIN-281) had no effect on Akt phosphorylation (Fig. 4g and h).

It is often the case that STAT3 phosphorylation leads to down-regulation of survivin.[7,8] Survivin is a member of the XIAP (X-linked inhibitor of apoptosis) group of proteins. Studies have shown that survivin works in a complex mechanism to promote cell growth and to inhibit apoptosis. Survivin is a component of the chromosomal passenger complex (CPC) and hence has a critical role cell cycle progression and cell proliferation.[9–12] Interestingly, **1** (KIN-1) and **6** (KIN-281) led to down-regulation of survivin in MDA-MB-468 (Fig. 4a and b) and MDA-MB-231 (Fig. 4c and d). The effect was sustained over the course of 48 h in both MDA-MB-468 and MDA-MB-231. Interestingly, both **1** and **6** also reduced expression of the pro-apoptotic protein Bcl-XL (Fig. 4a–d).

3.5. KIN-281 inhibits cell autophagy

A direct physical interaction between the anti-apoptotic proteins Bcl-2 or Bcl-XL and the autophagy regulator Beclin-1 was previously shown to inhibit autophagy in cancer cells.[13] In addition, it has been shown that STAT3 promotes autophagy through a complex with PKR.[14] Since **1** and **6** suppress Bcl-XL levels and inhibit STAT3 activation, we wondered whether treatment with these compounds had an effect on autophagic flux. To test this, levels of the processed LC3B, a widely used marker of autophagy[15] were measured in MDA-MB-231 and MDA-MB-468 cells following treatment with compound. Autophagic flux was evaluated by determining the levels of LC3B-I and LC3B-II by Western blot analysis in the presence or absence of the lysosomotropic agent bafilomycin A1 (BafA1) that inhibits autophagy at late stages. In both cases, we found that the compounds led to increased levels of LC3B-II (Fig. 5). Treatment of MDA-MB-468 cells with BafA1 resulted in substantial increase in LC3B-II compared to DMSO control consistent with there being robust autophagic flux in these cells at basal conditions. MDA-MB-231 cells showed a more modest increase in LC3B-II when treated with BafA1. Growth of cells at 1% oxygen (hypoxia) was used as a positive control for autophagy induction (lanes 5 and 6 in Fig. 5a and Fig. 5b). A pronounced increase in LC3B-II levels were detected in MDA-B-468 cells (lane 3 in Fig. 5a) and MDA-MB-231 cells (lane 3 in Fig. 5b) treated with compound. However, this was not further increased by co-treatment with BafA1 in either MDA-MB-468 or MDA-MB-231 cells suggesting that the compound was inhibiting autophagic flux and causing processed LC3B-II to accumulate.

4. Discussion

Here we test previously-identified quinazoline compounds in TNBC breast cancer cells and found them to inhibit cell viability and to impair colony formation in an anchorage-independent soft agar assay. The most potent among these compounds, namely **6** (KIN-281), inhibits several kinases with IC_{50}s of approximately 1 μM, including maternal embryonic leucine zipper kinase (MELK) and bone marrow X-linked (BMX). Studies have shown that both MELK and BMX are overexpressed in a number of tumors and their overexpression correlates strongly with patient outcome.[16–18] BMX is a member of the Tec non-receptor tyrosine kinase family. MELK has been identified as an important target for other epithelial tumors including colorectal, lung, breast, ovarian and brain.[3] High expression of MELK in cancer stem cells has also been found.[19,20] MELK is overexpressed in basal-like breast cancer and several studies have implicated the enzyme with tumor growth and metastasis.

[4,21] The inhibition of MELK, BMX and other kinases by **6** may explain its effect in TNBC cancer cells.

Some of the effects that we observed for **6** (KIN-281) may be partly associated with inhibition of MELK or BMX. MELK plays an important role in cell cycle.[22–25] Previous studies have shown that knockdown of MELK in U87 led to $p21^{WAF1/CIP1}$ up-regulation.[4] Interestingly, we found that our compounds up-regulated $p21^{WAF1/CIP1}$ in a time-dependent manner over 48 h. The down-regulation of cyclin A2 that is induced by the compounds is consistent with the effect on $p21^{WAF1/CIP1}$. Studies that have suggested that the effect on $p21^{WAF1/CIP1}$ is a p53-dependent process have been conflicting. One study has shown that MELK suppression has no effect on Ser15 phosphorylation in U87 or levels of p53, suggesting instead that the effect on p53 may be due to MDMX down-regulation rather than an effect on p53.[4] Another study found that suppressing MELK led to inhibition of Ser15 phosphorylation and increased stabilization of p53.[26] **1** (KIN-1) and **6** (KIN-281) had no effect on the levels of p53 in agreement with both studies. However, the compound inhibited Ser15 phosphorylation in a time-dependent fashion consistent with the results of Seong and coworkers.[26] We investigated the effect of the compounds on MDMX levels and observed an increase in MDMX, consistent with the observation of Seong and co-workers with MDM2.[26] **6** (KIN-281) does not affect p53 levels in MDA-MB-468 or MDA-MB-231 cells.

BMX is an intracellular non-receptor tyrosine kinase member of the Tec family of protein kinases. Like other Tec kinases, BMX possesses a membrane localization pleckstrin homology (PH) module along with a BH, SH3, SH2, and kinase domains that mediate protein-protein interactions and downstream signaling. BMX has been shown to directly associate and phosphorylate STAT3.[6] This process was found to be independent of JAK kinases, which are generally associated with STAT3 activation.[27] The inhibition BMX by **6** prompted us to explore whether STAT3 phosphorylation is affected in both MDA-MB-231 and MDA-MB-468. STAT proteins have dual roles: they transduce signals through the cytoplasm and function as transcription factors in the nucleus.[28,29] Following phosphorylation from specific tyrosine kinases, STATs form stable homodimers, sometimes heterodimers, through SRC homology 2 (SH2) domain interactions. In the nucleus, a STAT3 dimer complex bind to DNA and modulate the transcription of genes that play a critical role in promoting inflammatory and malignant processes. The effects on STAT3 went beyond merely inhibition of phosphorylation of the transcription factor. We found through EMSA that **1** (KIN-1) inhibited STAT3 DNA-binding. This suggests that the compound is likely also affecting STAT3 transcription factor activity. However, compound **6** had no effect on JAK kinases suggesting that inhibition of STAT3 occurs through another mechanism, possibly through PI3K by activation of BMX. A recent study has shown that phosphorylation of STAT3 in PI3K-transformed cells is driven by BMX.[6] The study demonstrates that instead of the usual PIP3/Akt/mTOR pathway, PIP3 leads to phosphorylation of BMX, which in turn phosphorylates STAT3 and leads to oncogenic phenotype (Fig. 6). In fact, we tested the effects of the compounds on Akt phosphorylation and found no effect confirming that the compound does not affect the PI3K/Akt/mTOR pathway.

We found that the compounds also suppressed the levels of pro-apoptotic survivin and Bcl-XL. Although survivin is often associated with apoptosis, it is a cell cycle protein that is highly up-regulated in cancer versus normal cells. Survivin has multiple functions. Initially thought to be strictly involved in programmed cell death, survivin has been shown to play a key role in cell cycle progression and cell proliferation. In fact, survivin is required for several stages of cell division. At metaphase, it localizes to kinetochores, then transfers to the central spindle mid-zone at anaphase, and finally accumulates in mid-bodies at telophase.[30] It physically associates with polymerized microtubules, mitotic chromatin-associated spindle microtubules, and the kinetochore-associated CPC through protein-protein interactions with Aurora B,[9,10] Borealin/Dasra B,[11] and Crm1.[12] Expression of survivin is controlled by several transcription factors including p53, FoxM1, and STAT3.

The effects of **6** on STAT3 levels and Bcl-XL prompted us to explore the effect of the compounds on cell autophagy. Bcl-XL forms a physical interaction with the BH3 domain of beclin-1.[31] Phosphorylation of beclin-1 by the CaMK member death-associated protein kinase 1 (DAPK1) leads to the disruption of the Bcl-XL·beclin-1 complex and subsequent increase in autophagy.[32] Previous studies have shown that STAT3 promotes autophagy through a complex with PKR (Fig. 6).[14] Autophagy is a highly conserved self-degradative process that plays a critical role in cellular stress response and survival mechanisms. Cells use autophagy to turnover damaged organelles, pathogens and large protein aggregates. This degradation process provides a critical source of amino acids, nucleotides, and fatty acids, especially for cancer cells, which are generally unable to acquire sufficient nutrients to sustain the ATP production required for these cells to survive. A commonly used marker for autophagy is LC3B-II.[15] We found that **6** (KIN-281) led to a significant increase in LC3-II levels suggesting that MELK may play a role in suppressing autophagy. The effects of the compound at 5 μM were as pronounced as bafilomycin A1, a well-known late-stage autophagy inhibitor. Inhibition of autophagy may have benefits for cancer treatment, particularly breast cancer where autophagy may help cells evade apoptosis.[33,34] Beyond cell survival, accumulating evidence suggests that autophagy is involved in nearly every step of the metastatic cascade. In fact, 50% of human breast cancers exhibit heterozygous deletion of beclin-1, which is critical for autophagosome formation.[35,36] By inhibiting autophagy, these compounds may thus have a beneficial effect for TNBC patients by limiting progression of disease.

Acknowledgments

The research was supported by the National Institutes of Health (CA135380) (SOM), the American Cancer Society Research Scholar Grant RSG-12-092-01-CDD (SOM), by the 100 Voices of Hope (SOM), and by the Indiana University School of Medicine Biomedical Research Grant (SOM).

References

1. Jamdade VS, Sethi N, Mundhe NA, Kumar P, Lahkar M, Sinha N. Br J Pharmacol. 2015;172:4228–4237. [PubMed: 26040571]
2. Mori S, Chang JT, Andrechek ER, et al. Oncogene. 2009;28:2796–2805. [PubMed: 19483725]
3. Gray D, Jubb AM, Hogue D, et al. Cancer Res. 2005;65:9751–9761. [PubMed: 16266996]
4. Kig C, Beullens M, Beke L, et al. J Biol Chem. 2013;288:24200–24212. [PubMed: 23836907]
5. Nakano I, Paucar AA, Bajpai R, et al. J Cell Biol. 2005;170:413–427. [PubMed: 16061694]

6. Guryanova OA, Wu Q, Cheng L, et al. Cancer Cell. 2011;19:498–511. [PubMed: 21481791]
7. Yu H, Kortylewski M, Pardoll D. Nat Rev Immunol. 2007;7:41–51. [PubMed: 17186030]
8. Basseres D, Baldwin A. Oncogene. 2006;25:6817–6830. [PubMed: 17072330]
9. Honda R, Körner R, Nigg EA. Mol Biol Cell. 2003;14:3325–3341. [PubMed: 12925766]
10. Wheatley SP, Carvalho A, Vagnarelli P, Earnshaw WC. Curr Biol. 2001;11:886–890. [PubMed: 11516652]
11. Gassmann R, Carvalho A, Henzing AJ, et al. J Cell Biol. 2004;166:179–191. [PubMed: 15249581]
12. Knauer SK, Bier C, Habtemichael N, Stauber RH. EMBO Rep. 2006;7:1259–1265. [PubMed: 17099693]
13. Mariño G, Niso-Santano M, Baehrecke EH, Kroemer G. Nat Rev Mol Cell Biol. 2014;15:81–94. [PubMed: 24401948]
14. Shen S, Niso-Santano M, Adjemian S, et al. Mol Cell. 2012;48:667–680. [PubMed: 23084476]
15. Klionsky DJ, Abdalla FC, Abeliovich H, et al. Autophagy. 2012;8:445–544. [PubMed: 22966490]
16. Nakano I, Masterman-Smith M, Saigusa K, et al. J Neurosci Res. 2008;86:48–60. [PubMed: 17722061]
17. Marie SK, Okamoto OK, Uno M, et al. Int J Cancer. 2008;122:807–815. [PubMed: 17960622]
18. Pickard MR, Green AR, Ellis IO, et al. Breast Cancer Res. 2009;11:R60. [PubMed: 19671159]
19. Ganguly R, Hong CS, Smith LGF, Kornblum HI, Nakano I. Mol Cancer Ther. 2014;13:1393–1398. [PubMed: 24795222]
20. Gu C, Banasavadi-Siddegowda YK, Joshi K, et al. Stem Cells. 2013;31:870–881. [PubMed: 23339114]
21. Wang Y, Lee Y-M, Baitsch L. eLife. 2014;e01763. [PubMed: 24844244]
22. Mirey G, Chartrain I, Froment C, et al. Cell Cycle. 2005;4:806–811. [PubMed: 15908796]
23. Seong H, Gil M, Kim K, Kim S, Ha H. Biochem J. 2002;361:597–604. [PubMed: 11802789]
24. Cordes S, Frank CA, Garriga G. Development. 2006;133:2747–2756. [PubMed: 16774992]
25. Davezac N, Baldin V, Blot J, Ducommun B, Tassan J-P. Oncogene. 2002;21:7630–7641. [PubMed: 12400006]
26. Seong H-A, Ha H. J Biol Chem. 2012;287:20797–20810. [PubMed: 22532570]
27. Rawlings JS, Rosler KM, Harrison DA. J Cell Sci. 2004;117:1281–1283. [PubMed: 15020666]
28. Yu H, Pardoll D, Jove R. Nat Rev Cancer. 2009;9:798–809. [PubMed: 19851315]
29. Song L, Turkson J, Karras JG, Jove R, Haura EB. Oncogene. 2003;22:4150–4165. [PubMed: 12833138]
30. Vagnarelli P, Earnshaw WC. Chromosoma. 2004;113:211–222. [PubMed: 15351889]
31. Maiuri MC, Le Toumelin G, Criollo A, et al. EMBO J. 2007;26:2527–2539. [PubMed: 17446862]
32. Zalckvar E, Berissi H, Mizrachy L, et al. EMBO Rep. 2009;10:285–292. [PubMed: 19180116]
33. Karantza V, White E. Autophagy. 2007;3:610–613. [PubMed: 17786023]
34. Ruddy SC, Lau R, Cabrita MA, et al. Mol Cancer Ther. 2014;13:1882–1893. [PubMed: 24785256]
35. Futreal P, Soderkvist P, Marks J, et al. Cancer Res. 1992;52:2624–2627. [PubMed: 1568230]
36. Saito H, Inazawa J, Saito S, et al. Cancer Res. 1993;53:3382–3385. [PubMed: 8100738]

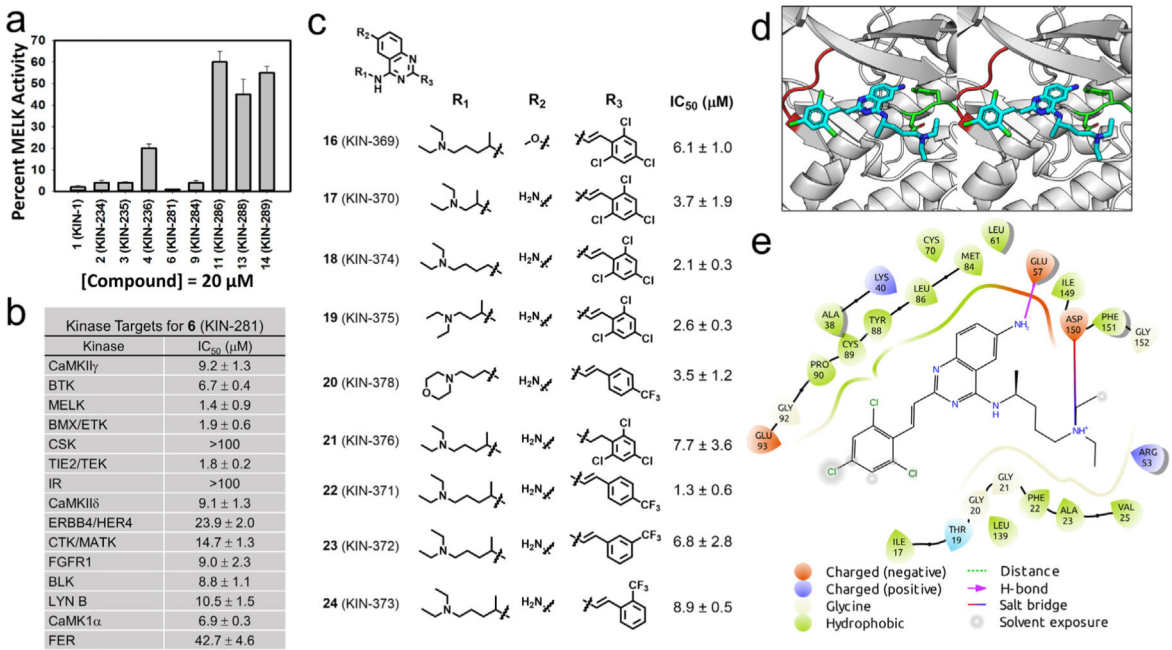

Fig. 1.

Small molecules inhibit MELK kinase. (a) Derivatives of **1** (KIN-1) were tested for inhibition of MELK activity at 20 μM; data shown as mean ± SD. (b) Compound **6** (KIN-281) was tested for its inhibition of 25 kinases that were selected from a previous kinome profiling. IC_{50}s were obtained for each kinase; data shown as mean ± SD. (c) Chemical structure of derivatives of **6** (KIN-281) that were synthesized along with IC_{50} for inhibition of MELK activity. (d) The binding mode of **6** (KIN-281, shown as cyan stick) to MELK (PDB: 4cqg, shown as gray cartoon). MELK is shown in cartoon, with the side chain of key residues shown in stick. The hinge loop and DFG motif of MELK are colored in red and green, respectively. The glycine-rich loop from Glu15 to Leu27 is removed to visualize the ATP binding site. In the model, the primary amine on the quinazoline core of the compound forms a hydrogen bond with Glu57 on the αC helix of the MELK (shown as dotted orange line). The N-alkylamine tail of the compound is stabilized by a salt bridge to Asp150 in the DFG motif of the kinase (shown as dotted green line). (e) A 2D view of the binding mode of (*S*)-**6** to MELK. Residues are shown as droplets, with the orientation of the droplet indicating the direction of the side chain of the given residue. The hydrogen bond between Glu57 and the quinazoline core is shown in magenta. The salt bridge between the N-alkylamine tail of the compound and Asp150 is shown as a line colored as a gradient from orange to blue. The ligand interaction diagram is generated using Schrödinger Maestro and a cutoff of 4 Å.

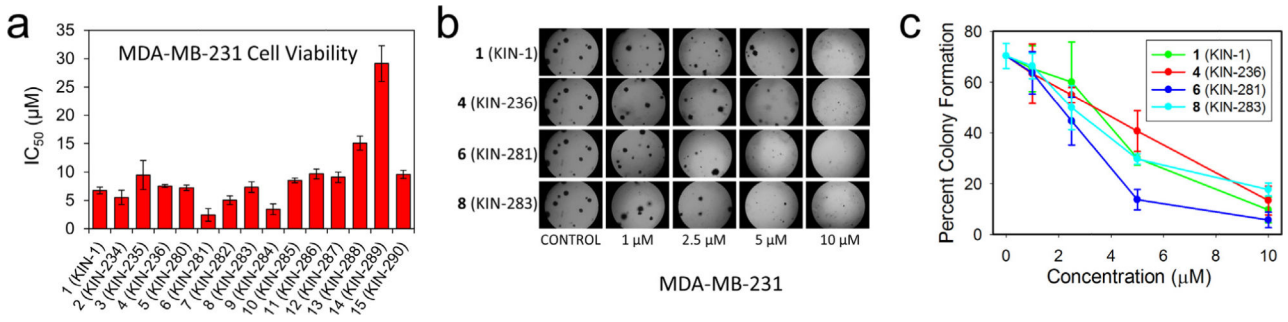

Fig. 2.

Compounds inhibits anchorage dependent and independent growth. (a) Effect of **1** (KIN-1) and derivatives on MDA-MB-231 measured by MTT over 3 days; data are shown as mean ± SD (n = 3) (b) Inhibition of anchorage-independent growth in MDA-MB-231 cancer cells (c) Quantification of data in (b); each value represents the mean ± SE taken from six different fields from two independent samples.

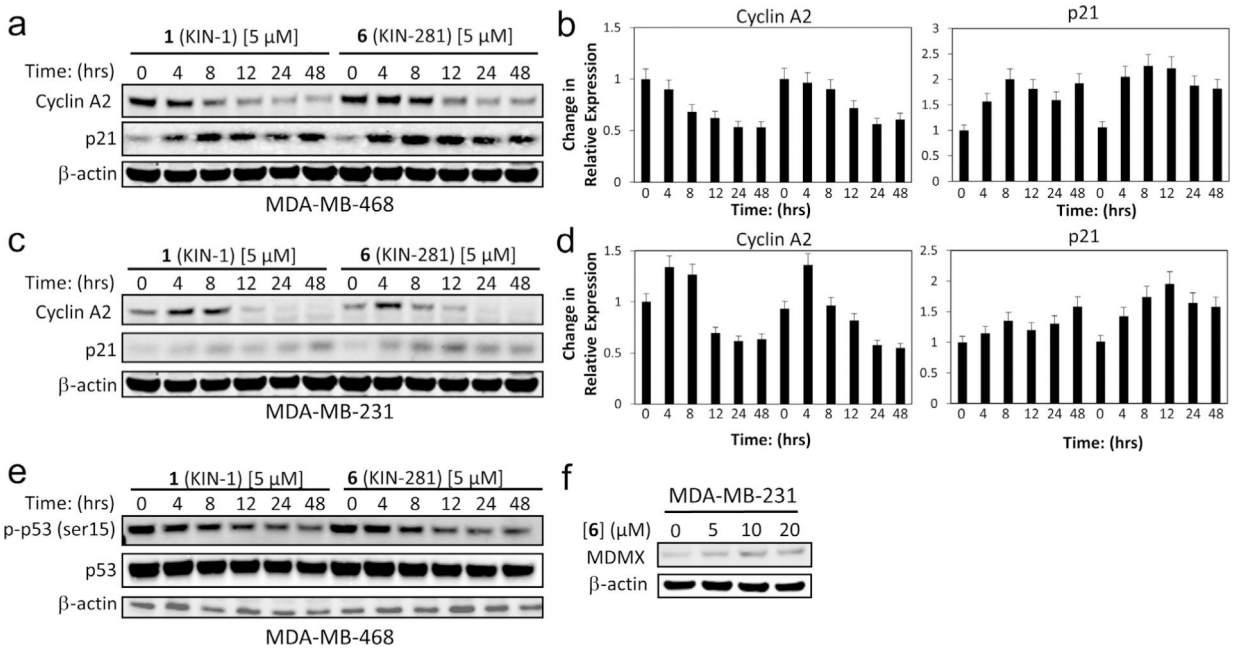

Fig. 3.

Compounds up-regulate p21. (a) Detection of cyclin A2 and p21 levels over the course of 48 h as a result of treatment MDA-MB-468 cells. β-actin serves as loading control. (b) Quantification of data shown in (a). The data are presented as percentage changes (mean ± SD; n = 2). (c) Detection of cyclin A2 and p21 levels in MDA-MB-231 cells following treatment with **1** (KIN-1) and **6** (KIN-281) over 48 h. Actin is used as loading control. (d) Quantification of data in (c); the data are presented as percentage changes relative to control (mean ± SD; n = 2). (e) Detection of p53 phosphorylation and p53 levels following treatment of MDA-MB-468 cells over 48 h. Actin is used as loading control. (f) Effect of increasing concentration of **6** on MDMX levels detected by immunoblot analysis following treatment of MDA-MB-231.

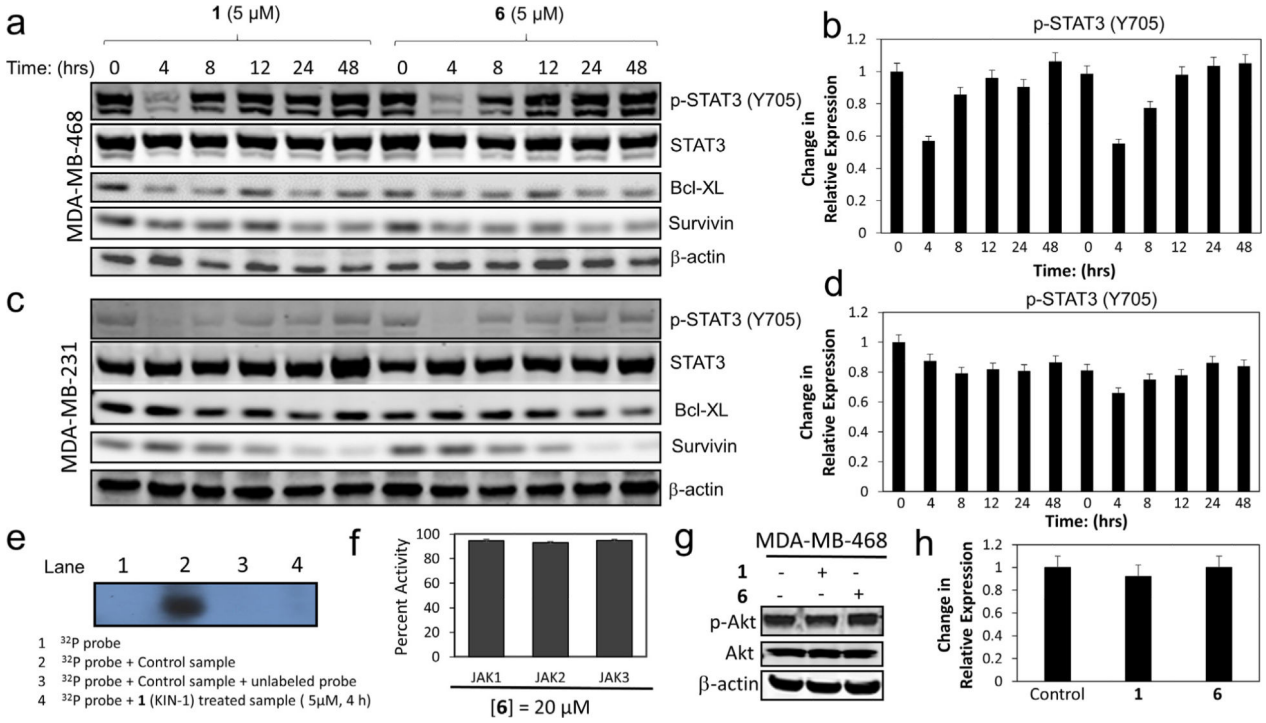

Fig. 4.

Compounds impair STAT3 phosphorylation and down-regulate pro-apoptotic Bcl-XL and survivin. (a) Effect of **1** (KIN-1) and **6** (KIN-281) on STAT3, Bcl-XL, and survivin levels as well as STAT3 phosphorylation analyzed by Western blot analysis at several time intervals over the course of 48 h in MDA-MB-468 cells. β-Actin is used as loading control. (b) Quantification of data in (a); the data are presented as percentage changes relative to control (mean ± SD; n = 2). (c) Effect of **1** (KIN-1) and **6** (KIN-281) on STAT3, Bcl-XL, and survivin levels as well as STAT3 phosphorylation analyzed by Western blot analysis at several time intervals over the course of 48 h in MDA-MB-231 cells. β-Actin is used as loading control. (d) Quantification of data in (a); the data are presented as percentage changes relative to control (mean ± SD; n = 2). (e) EMSA analysis to establish STAT3 binding to DNA; lane 1 is (f) Activity of **6** against JAK1, JAK2 and JAK3 kinases. (g) Western blot analysis of Akt phosphorylation as a result of treatment with **1**. (h) Quantification of data in (g); the data are presented as percentage changes relative to control (mean ± SD; n = 2).

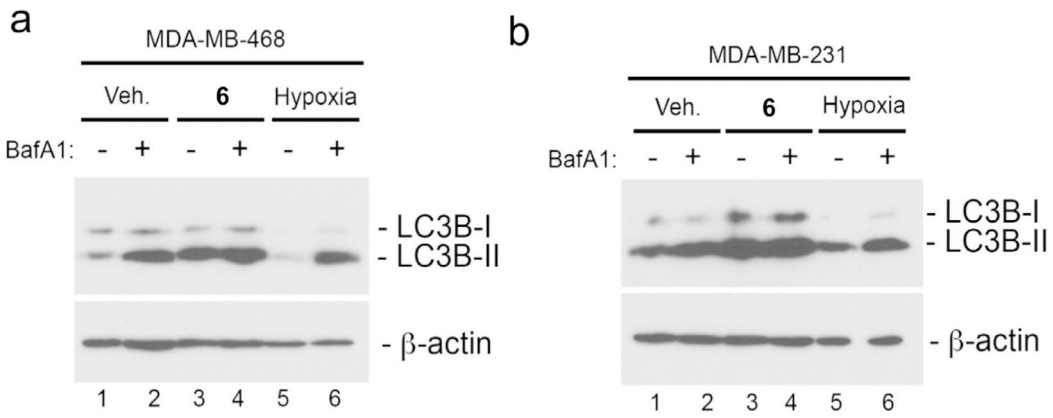

Fig. 5.

Compounds inhibit autophagy. Western blot analysis of LC3B-I and LC3B-II in MDA-MB-468 cells (a) and MDA-MB-231 cells (b) following treatment for 4 h in vehicle control (DMSO), 5 μM **6** (KIN-281) or at 1% oxygen. Bafilomycin A1 was added at 100 nM for the last 4 h of incubation to lanes 2, 4 and 6 as indicated.

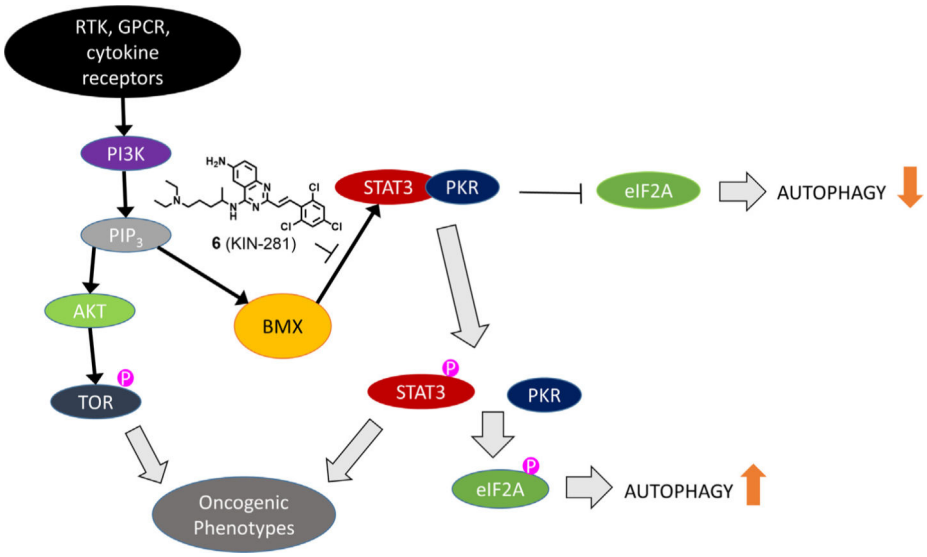

Fig. 6.

Schematic illustrating potential mechanism of action of KIN-281. Inhibition of BMX by the compound may be responsible for suppressing STAT3 activation through the PI3K pathway without affecting AKT. STAT3 activation leads to eIF2A phosphorylation and autophagy.

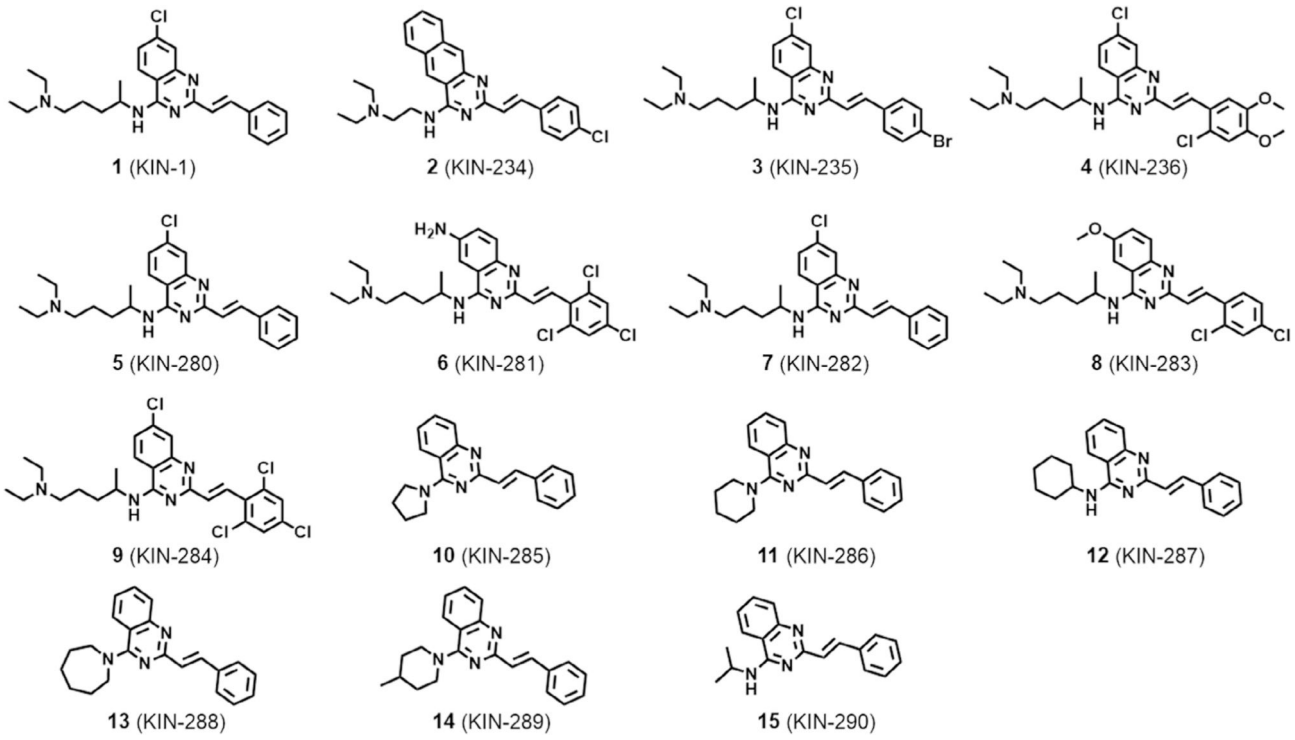

Scheme 1.

Chemical structure of active compounds identified from virtual screening.

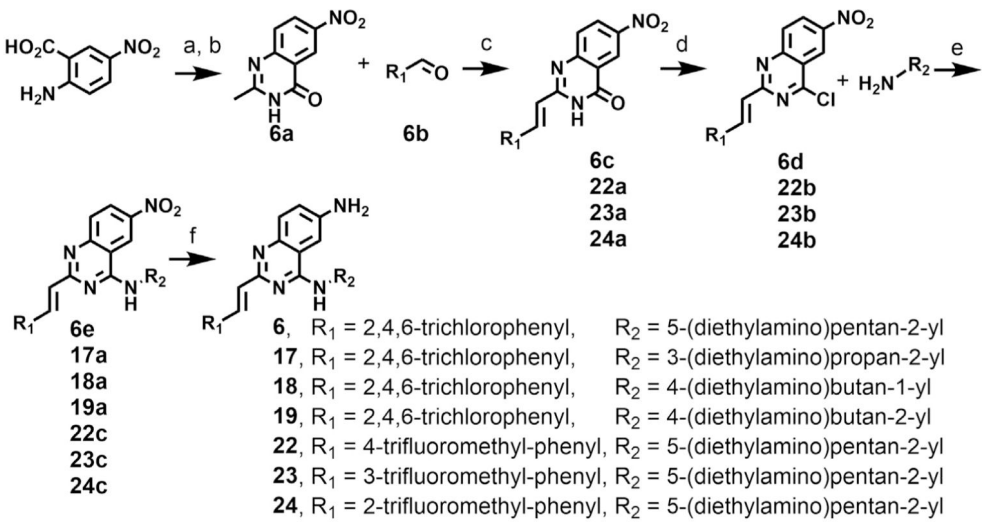

Reagents and conditions: (a) Ac_2O, 110 °C, 5 h; (b) $NH_3.H_2O$, 55 °C, 10 h; (c) AcOH, 110 °C, 30 h; (d) $POCl_3$, DIPEA, reflux; (e) THF, r.t., 3 h; (f) iron powder, NH_4Cl, H_2O-EtOH, reflux, 2 h.

Scheme 2.
Synthesis of derivatives of **6** (KIN-281).

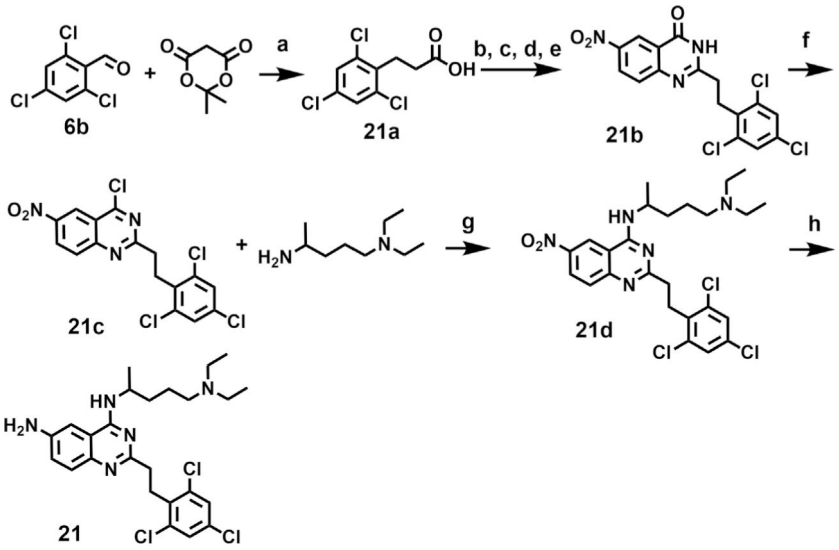

Scheme 3.
Synthesis of **21**.